An integrative modeling approach for the efficient estimation of cross sectional tibial stresses during locomotion

Timothy R. Derrick [a,*], W. Brent Edwards [b], Rebecca E. Fellin [c], Joseph F. Seay [c]

[a] Department of Kinesiology, Iowa State University, Ames, IA, USA
[b] Faculty of Kinesiology, University of Calgary, Calgary, Canada
[c] U.S. Army Research Institute of Environmental Medicine, Natick, MA, USA

ARTICLE INFO

ABSTRACT

The purpose of this research was to utilize a series of models to estimate the stress in a cross section of the tibia, located 62% from the proximal end, during walking. Twenty-eight male, active duty soldiers walked on an instrumented treadmill while external force data and kinematics were recorded. A rigid body model was used to estimate joint moments and reaction forces. A musculoskeletal model was used to gather muscle length, muscle velocity, moment arm and orientation information. Optimization procedures were used to estimate muscle forces and finally internal bone forces and moments were applied to an inhomogeneous, subject specific bone model obtained from CT scans to estimate stress in the bone cross section. Validity was assessed by comparison to stresses calculated from strain gage data in the literature and sensitivity was investigated using two simplified versions of the bone model-a homogeneous model and an ellipse approximation. Peak compressive stress occurred on the posterior aspect of the cross section (-47.5 ± 14.9 MPa). Peak tensile stress occurred on the anterior aspect (27.0 ± 11.7 MPa) while the location of peak shear was variable between subjects (7.2 ± 2.4 MPa). Peak compressive, tensile and shear stresses were within 0.52 MPa, 0.36 MPa and 3.02 MPa respectively of those calculated from the converted strain gage data. Peak values from a inhomogeneous model of the bone correlated well with homogeneous model (normal: 0.99; shear: 0.94) as did the normal ellipse model ($r = 0.89$–0.96). However, the relationship between shear stress in the inhomogeneous model and ellipse model was less accurate ($r = 0.64$). The procedures detailed in this paper provide a non-invasive and relatively quick method of estimating cross sectional stress that holds promise for assessing injury and osteogenic stimulus in bone during normal physical activity.

1. Introduction

In vivo stresses in lower extremity long bones are difficult to quantify experimentally and estimate computationally. However, these stresses represent the internal loading intensities within bone. They are dependent on the applied loading magnitude, bone structural geometry and material properties which play a fundamental role in skeletal injury and adaptation. One method of obtaining bone stress in vivo is the surgical attachment of strain gages directly to the bone (Milgrom et al., 2007) and subsequent calculation of stress (Lanyon et al., 1975). Another method is the application of finite element methods with bone models derived from advanced imaging techniques (Gray et al., 2008; Speirs et al., 2007). Strain gage analyses are limited to superficial, periosteal regions of bone, may produce localized pain or numbness in active subjects, and are often difficult to get approved by institutional review boards. Finite element methods often suffer from a lack of realistic boundary conditions and muscle forces, are relatively time consuming for subject-specific model generation, and can be computationally intensive when utilizing a clinically relevant sample size. A compromise may be a two-dimensional finite element model of a transverse cross section of bone at a specific area of interest. Three-dimensional forces and moments at the cross sectional centroid can be estimated using muscle and joint reaction forces obtained from a combination of experimentation and musculoskeletal modeling. A cross-sectional finite element model can then be used to estimate bone stress. This method allows for subject-specific bone geometry with inhomogeneous material properties, yet is simple, accurate and semi-automated enough to have potential in a clinical setting (Kourtis et al., 2008).

The selection of a particular bone model is dependent on the available equipment and may depend on the purpose of the research. Clinical computed tomography (CT) and peripheral

* Correspondence to: Iowa State University, 249 Forker Building, Ames, IA 50011, USA. Tel.: +1 515 294 8438; fax: +1 515 294 8740.
E-mail address: tderrick@iastate.edu (T.R. Derrick).

quantitative CT (pQCT) not only provide information about bone geometry, but also the apparent density distribution – necessary information for the construction of an inhomogeneous finite element model (Rho et al., 1995). However, these technologies expose individuals to varying degrees of ionizing radiation. On the other hand, magnetic resonance imaging (MRI) does not involve radiation and structural geometry can still be obtained but bone apparent density is not directly available. Advanced calibration techniques may allow MRI derived measurement of bone porosity which makes it possible to estimate apparent density (Hong et al., 2000). Both MRI and CT acquisition require expensive equipment with user rates of several hundred dollars per scan. A simple model of a bone cross section can be estimated without the use of these imaging techniques by modeling the bone geometry as an idealized hollow ellipse (Utz et al., 2009). Added subject specificity can be included in these models by directly measuring bone diameters from inexpensive radiographs (O'Neill and Ruff, 2004) or using group specific regression equations (Franklyn et al., 2008).

The purpose of this research was to develop and test an integrative modeling approach for the purpose of estimating tibial stresses (i.e., normal and shear) during locomotion without invasive techniques such as strain gages, or difficulties associated with subject-specific whole-bone finite element model generation. The tibia was chosen as the bone of interest, because it represents the location most prone to fatigue fracture in athletes (Sanderlin and Raspa, 2003) and military personnel (Milgrom et al., 1985) due to the large axial/bending loads it experiences during physical activity. The approximate junction of the middle and distal third of the tibial was chosen because it is the most prevalent site of stress fractures in adults (Sanderlin and Raspa, 2003). We hypothesized that restricting the location of stress estimation to the anteriomedial tibia, as used in previous strain gage studies, would substantially underestimate the peak stress magnitudes located elsewhere in the cross section. Also, we compared peak stress magnitudes from three different bone models of decreasing complexity. The first bone model consisted of a finite element mesh with geometry and inhomogeneous material properties derived from pQCT scans; the second model assumed identical geometry with homogeneous material properties assigned to each element (representing typical MRI data); the third model assumed bone cross sectional geometry to be an idealized hollow ellipse. We hypothesized that the simplified models would produce lower peak stress values than the inhomogeneous finite element mesh.

2. Methods

2.1. Protocol

Twenty-eight male, active duty soldiers (age: 20.5 ± 3.1 yr, mass: 85.4 ± 14.8 kg, height: 1.77 ± 0.08 m) volunteered and provided informed consent to participate in this research study. They walked on an instrumented treadmill (AMTI, Watertown, MA) for five minutes at 1.34 m/s and then external reaction forces and moments were collected at 2000 Hz. Retro-reflective markers were placed on the pelvis, right thigh, right leg and right foot to define the orientation of these segments. Markers located on the sacrum and both PSIS were used to define the pelvis and four-marker clusters were placed on the thigh, leg and foot. Additional anatomical markers were placed on both ASIS, medial and lateral condyles of the knee and medial and lateral malleoli of the ankle to help identify hip, knee and ankle joint centers. The hip joint center was calculated using the method of Bell et al. (1989) while knee and ankle joint centers were calculated using the mean of the medial and lateral markers at each joint. Markers were digitized at 200 Hz using a 10-camera Qualisys system, synchronized with the

instrumented treadmill. Five consecutive stance phases were selected for analysis with each stance phase classified as one trial of data.

2.2. Rigid body model

Segment masses were estimated using the regression equations of Dempster (1955) and segment moments of inertia and center of mass locations were estimated using the procedures of Hanavan (1964). Three-dimensional joint moments and reaction forces were estimated using inverse dynamics procedures. Data filtering was accomplished using the procedures of Edwards et al. (2011) to minimize artifact that can arise from differing analog and kinematic cutoff frequencies.

2.3. Musculoskeletal model

Joint angles derived from the marker data were used as input to a musculoskeletal model. This model was implemented in Matlab and used to estimate length and velocity adjusted maximal muscle forces, moment arms and insertion points for each of 44 lower extremity muscles during the stance phase of the walking cycle. Muscle parameters were obtained from Arnold et al. (2010). A maximal muscle velocity of 20 fiber lengths per second was assumed; muscle lengths were scaled to the length of the segments, and maximal isometric muscle forces were scaled to the masses of the individual subjects and then multiplied by 1.25 to account for the athletic subject pool. These maximal dynamic muscle force estimations were only used to constrain the optimization procedure.

2.4. Optimization

The joint moments derived from the rigid body model and the moment arms derived from the musculoskeletal model were used as inputs to a static optimization algorithm implemented in Matlab (fmincon function with the interior-point algorithm). The cost function (u) to be minimized was the sum of the squared muscle stresses (Glitsch and Baumann, 1997) and was subject to the constraints that 1) the internal moments calculated from the inverse dynamics were equal to the moments caused by the muscles and 2) the individual muscle forces were not less than zero nor greater than the maximal dynamic muscle forces estimated from the musculoskeletal model:

$$u = Min \sum_{i=1}^{44} \left[\frac{F_i}{A_i} \right]^2$$

Subject to: $r_{jk} \times F_i = M_{jk}$ and $0 \le F_i \le \text{Fmax}_i$

where F_i is the estimated muscle force of the ith muscle, A_i is the physiological cross sectional area of the ith muscle, r_{jk} is the muscle moment arm for each jth joint and kth plane of motion, M_{jk} is the joint moment for the jth joint and kth plane of motion, and Fmax_i is the maximal dynamic muscle force for the ith muscle. Note that not all planes of motion were utilized at all of the joints; only the sagittal plane hip, knee and ankle as well as frontal plane hip and ankle moments were included in the optimization.

2.5. Bone models

Inputs to the bone models were the 3D forces and moments acting at the centroid of the cross section of the bone. These loads were calculated by translating the effects of the knee joint contact force to the centroid location while subtracting the effects of muscles that insert proximal to the centroid. Centroid loads were
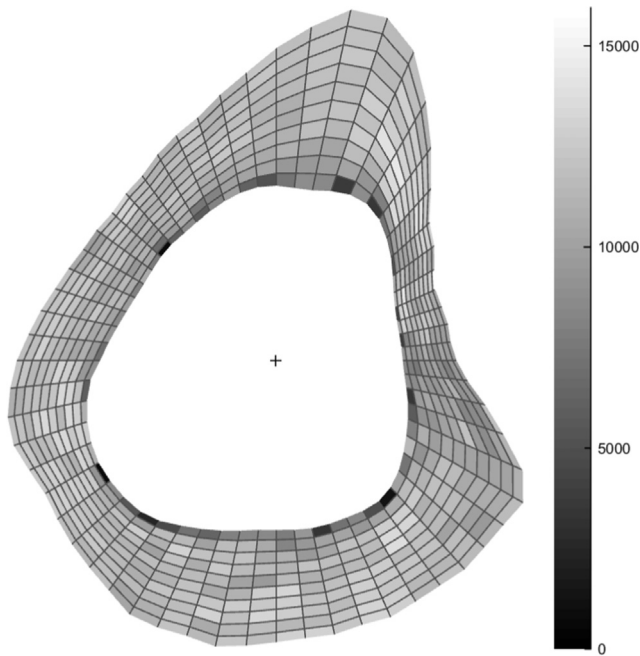
Fig. 1. 600 × 10 bone cross section mesh of the tibial at 62% from the proximal end. Values represent elastic moduli in MPa.

then distributed to the mesh elements before stresses were estimated.

Three subject-specific bone models of decreasing complexity were created for each subject. Information for each model was directly obtained from a pQCT scan at a cross section corresponding to 62% of the tibial length as measured from the proximal end of the tibia (Stratec XCT 3000, 60 kV,.4 mm resolution). The following 12 muscles cross this location: medial gastrocnemius, lateral gastrocnemius, soleus, tibialis posterior, flexor digitorum longus, flexor hallucis longus, tibialis anterior, peroneus brevis, peroneus longus, peroneus tertius, extensor digitorum longus and extensor hallucis longus. The models consisted of a finite element mesh with exact bone geometry and inhomogenous material properties (inhomogeneous model; IM), a finite element mesh with exact bone geometry and homogenous material properties (homogeneous model; HM), and a beam theory model with idealized geometry of a hollow ellipse (ellipse model; EM).

For the IM, pQCT images were read into Matlab using VA-BATTS subroutines (Kourtis et al. 2008, 2009). The software identified the periosteal and endosteal cortical boundaries, created a finite element mesh of the bone geometry (10 radial nodes, 60 circumferential nodes), and converted the CT attenuation values (att) to bone apparent density (ρ), and then to elastic moduli (E) (Fig. 1). The Poison ratio was 0.3 (Wirtz et al., 2000).

$\rho = 1484*att-322$, (machine specific equation provided by manufacturer)

$E = -3.842 + 0.013\rho$ (Rho et al., 1995)

Internal bone forces and moments for each footfall were distributed among the elements of mesh to obtain normal and shear stresses in each element using inhomogeneous beam theory and the finite element method (FEM), respectively (Kourtis et al., 2008, 2009).

The HM shared an identical finite element mesh with the IM, but a constant elastic moduli was assigned to each element that was equal to the average E from the IM. The HM was used to simulate a model obtained from a typical MRI scan with addition information about the average cortical bone density of the cross section.

The EM was constructed from the inner and outer radii of the bone outlines in the anterior-posterior and the medial-lateral directions. Basic beam theory was used to estimate the normal stresses at the vertices, and therefore no assumptions concerning bone elastic moduli were needed for this model; shear stresses were not presented.

2.6. Analysis

The stance phase of five successive footfalls were analyzed for each subject. Internal bone forces and moments were examined for their relative contributions to peak stress as were reaction forces and muscle forces. Normal stress was analyzed at the location of peak tension, peak compression and at a location on the anterior-medial periphery of the cross section. This latter location was chosen to represent a virtual strain gage to facilitate comparisons with an anisotropic stress analysis (Carter, 1978) of rosette strain gage data (Lanyon et al., 1975). These data were collected from a 35-year old male with no shoes walking at 1.4 m/s. Sensitivity to the location of this virtual strain gage was established by moving the location one element clockwise (1.27 mm) and noting the change in stress. Shear stress was also calculated at the virtual strain gage location but only so that a comparison could be made with the Carter/Lanyon data. Peak tensile and compressive stress from the IM and HM homogeneous finite element models as well as the simplified hollow ellipse model were compared using paired t-test statistics (alpha=0.05). Correlations between the stresses derived at the virtual strain gage location and those at the locations of peak compression and tension were used to examine the utility of using strain gage data to estimate injury potential.

3. Results

3.1. Internal bone forces and moments

Peak axial forces acting on the centroid of the cross section 62% from the proximal end of the tibia occurred at 75.5 ± 1.9% of stance (Fig. 2A). The majority of the axial force during peak loading was the result of muscular contractions (80.5 ± 2.1%), while the remaining force was due to the axial component of the joint reaction force. The joint reaction force and the muscles also produced moments acting at the centroid of the cross section. During peak loading the moment generated by the reaction force tended to bend the tibia in a concave anterior direction (−0.078 ± 0.009 BWm) while the moment generated by the muscles tended to bend the tibia in a concave posterior direction (0.153 ± 0.018 BWm) (Fig. 2B). The result of these two moments was a net moment (0.076 ± 0.015 BWm) that tended to bend the tibia in a concave posterior manner.

3.2. Cross sectional stress

The resultant axial forces and bending moments produced peak tension on the anterior aspect of the IM tibial cross section (27.0 ± 11.7 MPa) and peak compression on the posterior aspect (−47.5 ± 14.9 MPa). Peak tension occurred at a location on the periphery of the cross section that was an average of 67.0 ± 8.5° from the lateral axis in a counter-clockwise direction (Fig. 3); peak compression occurred at 251.1 ± 15.9°. The bending moments were responsible for 71.8 ± 5.0% of the peak compressive stress. The axial components of the reaction and muscle forces produced compression on the entire cross section and comprised the remainder of the peak compressive stress. Torsional load accounted for 98.3 ± 3.1% of the peak shear stress in the cross section.
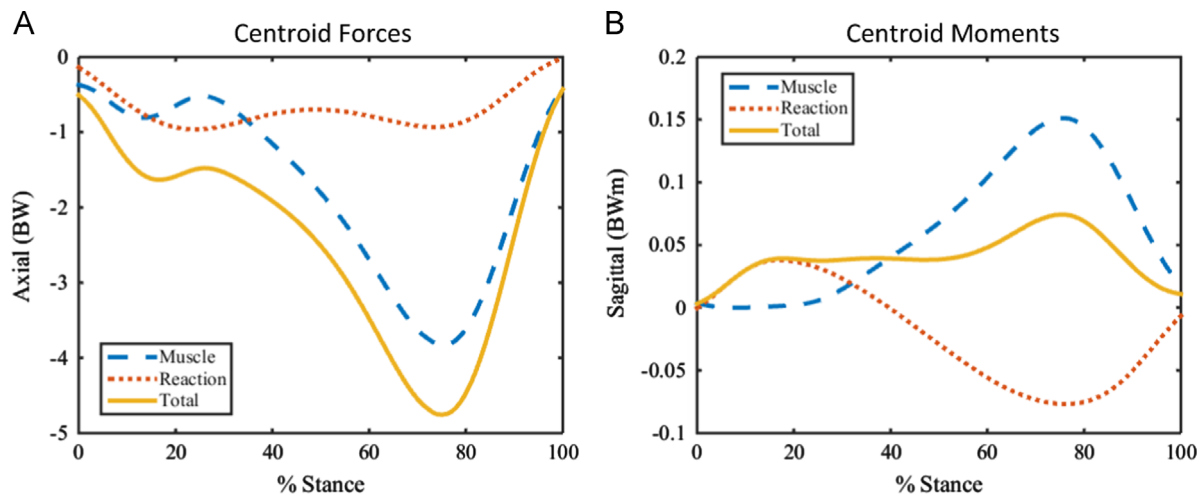
Fig. 2. Axial forces (A) and sagittal moments (B) acting at the centroid of the cross section 62% from the proximal end of the tibia while walking. The total force/moment is a sum of the muscle and reaction components. Negative axial forces indicate compression and positive axial forces indicate tension. Negative moments indicate bending in a concave posterior manner and positive moments indicate bending in a concave anterior manner.
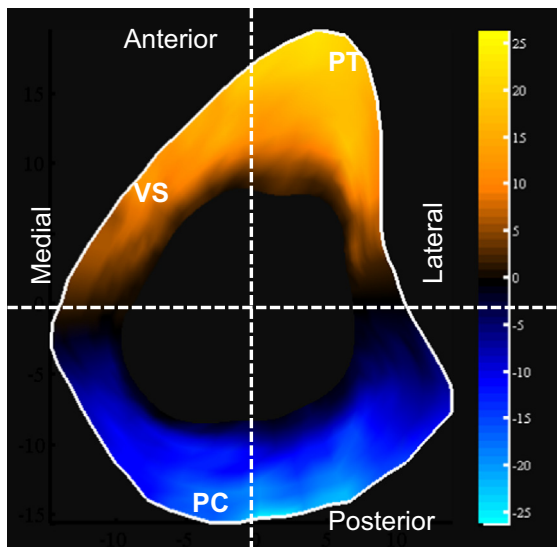

Fig. 3. Representative right tibia cross section at 62% from the proximal end at the time of peak compressive stress. Positive values indicate tensile stress and negative values compressive stress. "VS" indicates location of the virtual strain gage. "PT" indicates the typical location of peak tension and "PC" indicates the typical location of peak compression. Units are MPa.
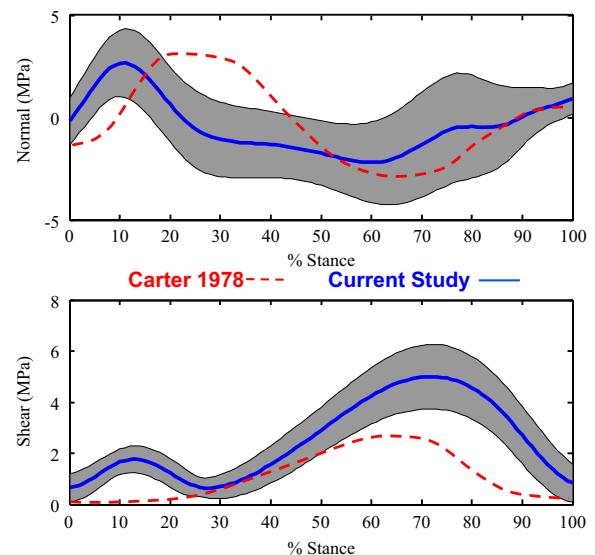

Fig. 4. A comparison of the virtual strain gage normal and shear stress (solid lines with 1 standard deviation shaded region) and the stresses calculated by Carter (1978) from a single subject with a strain gage on the anterior-medial aspect of the tibia (dashed lines).

Peak shear stress was 7.3 ± 2.4 MPa, but the location of the peak value was dependent on the individual shape of the bone and thus quite variable between subjects ($118.8 \pm 142.7°$).

3.3. Stress at the virtual strain gage location

Stress located at a region of the cross section approximating a location of strain gage attachment (Fig. 3) was substantially less than the peak stress of the cross section owing to its proximity to the neutral axis of bending. The average stresses at the virtual strain gage location from the current study compared well with the strain gage derived calculations of stress from Carter (1978) (Fig. 4). Peak tensile stress (current: 3.08 ± 1.80 MPa, Carter: 3.6 MPa) occurred during weight acceptance and peak compressive stress (current: -2.94 ± 1.69 MPa, Carter: -3.3 MPa) occurred during pushoff. Peak transverse stress was greater than that of Carter (current: 5.19 ± 1.34 MPa, Carter: 2.1 MPa) but occurred at approximately the same instance of stance.

Stress estimation was highly sensitive to the location of the virtual strain gage location. Moving the virtual strain gage 1.27 mm clockwise (away from the neutral axis) along the periphery of the cross section increased the peak tensile stress from 3.08 MPa to 4.11 MPa and decreased the magnitude of the peak compressive stress from -2.94 MPa to -1.67 MPa. These are changes of 33% and 58% for the tensile and compressive stresses respectively for a 1.27 mm change in location of the virtual sensor. Correlations between the peak stresses measured at the virtual strain gage location and the overall peak stresses were $-.06$ for compression and .13 for tension.

3.4. Alternative models

The relationship between the models is shown in the scatter plots of Fig. 5. Although peak tensile stress was not significantly different between the IM and the HM, peak compressive stress in the HM was 6.3% less than the IM model and peak shear was 5.9% less (Table 1B). Correlations between the IM and HM were $r=0.99$
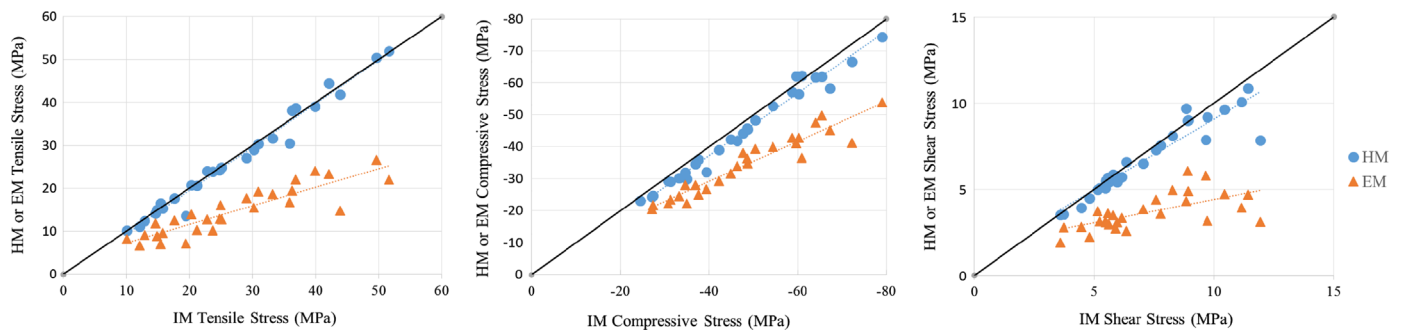
Fig. 5. Scatter plots showing the relationship between peak stress values using the inhomogeneous model (IM) vs the homogeneous model (HM) and the ellipse model (EM). Dashed lines indicate the linear trends. Solid lines represent a perfect relationship.
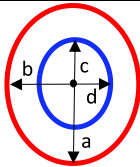
Table 1
A comparison of the inhomogeneous model to the simpler homogeneous and the hollow ellipse models. Part A shows the mean ± standard deviation of the outer (ro) and inner (ri) radii in the anterior-posterior (ap) and the medial-lateral (ml) directions. Part B shows the means, standard deviations and correlations (r) with the inhomogeneous model.
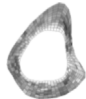
A.		
a) roap (mm)	17.3 ± 1.8	
b) roml (mm)	13.7 ± 1.1	
c) riap (mm)	10.4 ± 1.8	
d) riml (mm)	9.9 ± 1.2	

B.	CT Model	Homogeneous Model		Hollow Ellipse Model	
	mean±sd	mean±sd	r w/CT model	mean±sd	r w/CT model
cortical area (mm^2)	356.7 ± 47.0	356.7 ± 47.0	1.00	420.7 ± 64.4	0.91
peak anterior tension (MPa)	27.0 ± 11.7	26.5 ± 11.9	0.99	14.6 ± 5.7	0.89
peak posterior compression (MPa)	-47.5 ± 14.9	-44.5 ± 14.7	0.99	-33.8 ± 9.7	0.96
peak shear (MPa)	7.2 ± 2.4	6.8 ± 2.1	0.94	3.6 ± 1.0	0.64

Notes: the homogeneous model was significantly different from the CT model in compression and shear but not tension. The hollow ellipse model was statistically different from the CT model in compression, tension. shear and area.

for the peak tensile stress and $r=0.99$ for the peak compressive stress. The EM was defined by two outside radii and 2 inside radii (Table 1A). The area estimated by the elliptical model significantly overestimated the cross sectional area of the bone and therefore significantly underestimated the peak stresses when compared the IM (tensile: 28.9%; compressive: 45.7%; shear: 49.3%). However, the correlations between the IM and the EM were $r=0.91$ for the cortical area, $r=0.89$ for the peak tensile stress, and $r=0.96$ for the peak compressive stress (Table 1B). The peak shear correlation between the IM and EM was much lower ($r=0.64$).

4. Discussion

The quantification of in vivo tibial stress has usually involved either direct measurement through strain gage instrumentation and subsequent conversion to stress values or estimation through finite element modeling of the entire bone. Other researchers have attempted direct comparison of modeled results with in vivo

strain measurements with good success. Al Nazer et al. (2011) used realistic reaction forces and forces from ten muscles with an MRI derived bone model to estimate tibial strains for four walking cycles of a single subject. The advantages of the current research is that it used a musculoskeletal model consisting of 44 muscles, it used subject specific inhomogeneous bone models, procedures were simple and fast enough to estimate loading on 28 subjects, and the locations of peak compressive and tensile loading were reported. This is a non-invasive and relatively quick method that holds promise for the analysis of large amounts of data because it can be mostly automated. On average the IM model stress analysis for one footfall took about 2 min to complete (Intel i5 CPU, 3.2 GHz).

Increasing the number of models in a study increases the number of assumptions that must be made. In short, the inverse dynamics analysis assumes that the human body acts as a series of rigid bodies connected by frictionless joints, the musculoskeletal model assumes that the muscles can be defined by a series of straight lines and have attachments at discrete points, the

optimization technique assumes muscle recruitment is accomplished in a way that minimizes the sum of the squared stresses in the muscles, and the bone models assume that the moments and forces act at the centroid of the bone. In addition, the bone models assume that the influence of the fibula is minimal. Rather than test each of these assumptions individually, the results of this study were compared to the strain gage data that were converted to stresses from the literature.

Locations of the peak magnitudes of the stresses in this study showed agreement with our current understanding of stress fractures and previous strain gage research. The locations of peak compressive (251.1°) and tensile (67.0°) stresses agreed with the orthopaedic literature. For instance, Boden et al. (2001) suggested that the most common stress fractures in the tibia occur on the posteromedial or compression side and although anterior fractures are less common they exhibit poorer healing properties as would be expected from tensile fractures. The calculated normal and shear stress compared well with the converted strain gage data of Carter/Lanyon but our data highlight the difficulty in attempting to interpret stresses at a location (135°) so close to the neutral axis. Only 11.4% and 6.1% of the peak tensile and compressive stress are present at the location of the strain gage. This led to poor correlations between strain gage derived stress and the actual peak stress in the bone.

A comparison of the three bone models suggests that simplifications can be made without substantially altering the conclusions of within subject experimental designs. In addition to detailed geometry, the IM incorporates the heterogeneity of the bone material, which should, in theory, provide the most accurate results. However, the IM requires small amounts of ionizing radiation and relatively expensive equipment to obtain the data for the inhomogeneous CT model. The HM eliminates variation in bone density within the cortical bone but it retains the geometry of the cross section. These data could be obtained from an MRI scan as long as the average density of the cortical bone in the cross section is known. Radiation would be eliminated with MRI scans. With correlations of $r=0.94$ to 0.99 there is little loss of information. If neither CT nor MRI scans are available it is still possible to estimate the peak tensile and compressive stresses using the hollow ellipse model. The subject specific ellipse models that we used require good estimates of the inner and outer radii in the anterior-posterior and the medial-lateral directions. These estimates could be obtained from quality sagittal and frontal radiographs. In the absence of individual radii data there are studies that estimated these radii in the tibia (Franklyn et al., 2008; Gray et al., 2008). The correlations between the hollow ellipse model and the CT model were 0.89–0.96 for normal stress but only 0.64 for the shear stress. In addition, the absolute difference in the models was substantial. Caution is emphasized if using this method to determine differences between groups of subjects.

Triceps surae activity tends to reduce tibial bending and equalize injury potential within this cross section. Walking axial forces and moments in the mid-tibia are predominantly the result of triceps surae muscle activity and reaction forces. The moments caused by these two sources bend the bone in opposite directions during peak compressive stress so it could be considered that the triceps surae provide some amount of protection by countering the bending caused by the reaction force. Both muscle and reaction forces compress the entirety of the tibial cross section while the resulting moment compresses the posterior aspect and produces tension on the anterior aspect. The net result of both the axial force and the moment is a high posterior compression and a somewhat lower anterior tension. But, tensile and compressive stresses are not equivalent in terms of their proximity to failure. Ultimate strength in human bone is approximately 193 MPa for compression and 133 MPa for tension (Reilly and Burstein, 1975).

As a percent of ultimate strength the compressive stresses in this study were only slightly greater than the tensile stresses (25.0% for compression and 20.3% for tension) giving a factor of safety of 4–5.

Stress and strain within biological tissue of the body represent the best possible information to assess injury potential. Not only do stress distributions incorporate information about the load experienced by the body but they also represent the state of the biological material. Forces and moments acting on a smaller cross section of the bone will result in greater stress values. Since failure of the material can result from either loads that are too high or materials that are too weak, it is important to consider the combined effect of forces and material when studying injury potential.

Conflict of interest statement

There are no financial or personal relationships with other people or organizations that could inappropriately influence this work.

Acknowledgements/Disclaimer

References

Al Nazer, R., Klodowski, A., Rantalainen, T., Heinonen, A., Sievänen, H., Mikkola, A., 2011. A full body musculoskeletal model based on flexible multibody simulation approach utilized in bone strain analysis during human locomotion. Comput. Methods Biomech. Biomed. Eng. 14 (06), 573–579.

Arnold, E.M., Ward, S.R., Lieber, R.L., Delp, S.L., 2010. A model of the lower limb for analysis of human movement. Ann. Biomed. Eng. 38 (2), 269–279.

Bell, A.L., Pederson, D.R., Brand, R.A., 1989. Prediction of hip joint center location from external landmarks. Hum. Mov. Sci. 8 (1), 3–16.

Boden, B.P., Osbahr, D.C., Jimenez, C., 2001. Low-risk stress fractures. Am. J. Sports Med. 29 (1), 100–111.

Carter, D.R., 1978. Anisotropic analysis of strain rosette information from cortical bone. J. Biomech. 11, 199–202.

Dempster, W.T., 1955. Space requirements of the seated operator: Geometrical, kinematic, and mechanical aspects of the body with special reference to the limbs (Wright Air Development Center Tech. Rep. No. 55-159). Dayton, OH: Wright-Patterson Air Force Base, WADC. (National Technical Information Service No. AD-087892).

Edwards, W.B., Troy, K.L., Derrick, T.R., 2011. On the filtering of intersegmental loads during running. Gait Posture 34 (3), 435–438.

Franklyn, M., Oakes, B., Field, B., Wells, P., Morgan, D., 2008. Section modulus is the optimum geometric predictor for stress fractures and medial tibial stress syndrome in both male and female athletes. Am. J. Sports Med. 36 (6), 1179–1189.

Glitsch, U., Baumann, W., 1997. The three-dimensional determination of internal loads in the lower extremity. J. Biomech. 30, 1123–1131.

Gray, H.A., Taddei, F., Zavatsky, A.B., Cristofolini, L., Gill, H.S., 2008. Experimental validation of a finite element model of a human cadaveric tibia. J. Biomech. Eng. 130 (3), 031016.

Hanavan Jr, E.P., 1964. A mathematical model of the human body (No. AFIT-GA-PHYS-64-3). Air Force Aerospace Medical Research Lab Wright-Patterson Afb OH.

Hong, J., Hipp, J.A., Mulkern, R.V., Jaramillo, D., Snyder, B.D., 2000. Magnetic resonance imaging measurements of bone density and cross-sectional geometry. Calcif. Tissue Int. 66 (1), 74–78.

Kourtis, L.C., Carter, D.R., Kesari, H., Beaupré, G.S., 2008. A new software tool (VA-BATTS) to calculate bending, axial, torsional, and transverse shear stresses within bone cross sections having inhomogeneous material properties. Comput. Methods Biomech. Biomed. Eng. 11 (5), 463–476.

Kourtis, L., Kesari, H., Carter, D., Beaupré, G., 2009. Transverse and torsional shear stresses in prismatic bodies having inhomogeneous material properties using a new 2D stress function. J. Mech. Mater. Struct. 4 (4), 659–674.

Lanyon, L.E., Hampson, W.G.J., Goodship, A.G., Shah, J.S., 1975. Bone deformation recorded in vivo from strain gauges attached to the human tibial shaft. Acta Orthop. Scand. 46, 256–268.

Milgrom, C., Giladi, M., Stein, M., Kashtan, H., Margulies, J.Y., Chisin, R., Steinberg, R., Aharonson, Z., 1985. Stress fractures in military recruits. A prospective study showing an unusually high incidence. J. Bone Jt. Surg. Br. 67 (5), 732–735.

Milgrom, C., Radeva-Petrova, D.R., Finestone, A., Nyska, M., Mendelson, S., Benjuya, N., Burr, D., 2007. The effect of muscle fatigue on in vivo tibial strains. J. Biomech. 40 (4), 845–850.

O'Neill, M.C., Ruff, C.B., 2004. Estimating human long bone cross-sectional geometric properties: a comparison of noninvasive methods. J. Hum. Evol. 47 (4), 221–235.

Reilly, D.T., Burstein, A.H., 1975. The elastic and ultimate properties of compact bone tissue. J. Biomech. 8 (6), 393–405.

Rho, J.Y., Hobatho, M.C., Ashman, R.B., 1995. Relations of mechanical properties to density and CT numbers in human bone. Med. Eng. Phys. 17 (5), 347–355.

Sanderlin, B.W., Raspa, R.F., 2003. Common stress fractures. Am. Fam. Physician 68 (8), 1527–1532.

Speirs, A.D., Heller, M.O., Duda, G.N., Taylor, W.R., 2007. Physiologically based boundary conditions in finite element modelling. J. Biomech. 40 (10), 2318–2323.

Utz, J.C., Nelson, S., O'Toole, B.J., van Breukelen, F., 2009. Bone strength is maintained after 8 months of inactivity in hibernating golden-mantled ground squirrels, Spermophilus lateralis. J. Exp. Biol. 212 (17), 2746–2752.

Wirtz, D.C., Schiffers, N., Pandorf, T., Radermacher, K., Weichert, D., Forst, R., 2000. Critical evaluation of known bone material properties to realize anisotropic FE-simulation of the proximal femur. J. Biomech. 33 (10), 1325–1330.